

Kerr rotation signature of nonlinear Maxwell electrodynamics under a uniform electromagnetic background

M. J. Neves^{a*} and Pedro D. S. Silva^{b†}

^a*Departamento de Física, Universidade Federal Rural do Rio de Janeiro,
BR 465-07, CEP 23890-971, Seropédica, RJ, Brazil and*

^b*Coordenação do Curso de Ciências Naturais - Física, Universidade Federal do Maranhão,
Campus de Bacabal, Bacabal, Maranhão, 65700-000, Brazil*

Nonlinear electrodynamics naturally arises in quantum field theory, where the electromagnetic vacuum behaves as an effective nonlinear optical medium, leading to phenomena such as vacuum birefringence and dichroism. Among the recently proposed models, modified Maxwell electrodynamics (ModMax) stands out as a conformally invariant nonlinear extension of Maxwell theory that preserves the fundamental symmetries of classical electrodynamics while predicting nontrivial optical effects. In this work, we investigate optical effects in ModMax electrodynamics in the presence of an external electromagnetic field. Considering uniform and constant magnetic and electric backgrounds, the solutions for the refractive indices are revisited. Using these results, we obtain the propagating modes and the phase shift (birefringence) for plane wave solutions in the presence of a pure magnetic background field. Afterwards, we investigate the Goos–Hänchen effect considering the interface between a simple dielectric and a medium whose electromagnetic response tensors are ruled by the ModMax electrodynamics. Further, based on the general reflection problem, we discuss the complex Kerr rotation with both the electric (E) and magnetic (B) background fields, considering two main cases: i) $B > E$ and ii) $E > B$. Our findings indicate that the γ parameter and the ratios (B/E) and (E/B) play a central role in describing the Kerr signals (rotation and ellipticity) of systems with optical effects induced by nonlinear electromagnetic interactions.

I. INTRODUCTION

Vacuum can be regarded as a nonlinear optical medium, a concept that naturally emerges in the Standard Model of elementary particles [1]. In this context, nonlinear electrodynamics models may exhibit phenomena such as vacuum dichroism and birefringence. In particular, vacuum magnetic birefringence (VMB) is a macroscopic quantum effect predicted by quantum electrodynamics (QED) [2, 3], in which the refractive indices for light polarized parallel and perpendicular to an external magnetic field differ in a nontrivial way. The PVLAS (Polarisation of Vacuum with LASER) experiment devoted 25 years of continuous effort to the search for vacuum birefringence and dichroism. Although it has not yet reached the sensitivity required to observe the QED-predicted values, it has established the most stringent experimental bounds to date [4–7]. While VMB has not been directly detected in laboratory conditions, indirect evidence has been reported in the neutron star RX J1856.5 – 3754, which possesses magnetic fields on the order of 10^{13} Gauss [8].

Originally, the first non-linear electrodynamics (ED) was proposed by M. Born and L. Infeld to explain the static electric field of a pointlike charge particle at the origin [9]. Some years later, W. Heisenberg and H. Euler obtained the effective lagrangian for fermions interacting with an external electromagnetic field in QED, which leads to non-linear effects from quantum corrections at

one loop [2]. Thereby, these are the two most well-known non-linear EDs in the literature. After some decades, there are many others examples of non-linear EDs that includes several applications in research areas as: Superstring theories [10, 11], Black hole solutions [12, 13], Magnetic Monopoles [14], Physics beyond the Standard Model [15], Material physics [16], Axion physics [17, 18], Plasma [19, 20], and others [21–31]. A new non-linear electrodynamics that preserves all the symmetries, including the conformal invariance, has been proposed and is known in the literature as modified Maxwell electrodynamics (ModMax) [32, 33]. The ModMax ED is also a possible solution for black holes [34], contains connection with supersymmetry [35], Brane physics [36], and exhibits the birefringence effect [37]. Since the ModMax is a relatively new non-linear ED, it motivates us to investigate other optical phenomena beyond the birefringence, such as the Goos–Hänchen effect [38], polarization rotation, and the complex Kerr rotation.

The reflection of light on surfaces constitutes a useful way for investigating the properties of distinct media, including the generation of circularly polarized and elliptically polarized waves, which are not commonly available in nature [39]. These polarization states may emerge upon reflection from materials characterized by a complex refractive index (such as metals and chiral media) or under conditions of total internal reflection.

When an incident electromagnetic wave impinges on the surface of a gyrotropic medium, the reflected wave generally becomes elliptically polarized. The resulting polarization angles (rotation and ellipticity) define the Kerr rotation [41–43], which is extensively employed to probe the optical and magneto-optical properties of

* mariojr@ufrj.br

† pedro.dss@ufma.br

materials. For instance, in Weyl semimetals [44–46], where the axion term yields non-trivial optical responses (frequency-dependent Kerr signals) [47]. These properties have been identified as relevant aspects in optical devices, such as chiral filters, circular polarizers, and optical isolators, since one can prevent the propagation of RCP and LCP waves within selected frequency intervals [48, 49].

In most material systems, however, Kerr rotations are typically small, amounting to less than 1 degree in conventional materials [50] and lying in the range of 10^{-6} to 10^{-4} radians for topological insulators [51]. The analysis of Kerr rotation has also served as an important diagnostic tool in the investigation of diverse physical systems, including precision measurements in quantum systems [52], unconventional superconductors [53], and media described within CPT-even Lorentz-symmetry-violating electrodynamics [54].

Most recently, optical signatures of axion dielectrics have been reported [55], where the chiral magnetic conductivity enables several effects, such as partial Brewster angles for polarization control, Goos-Hänchen shift, giant Kerr signals, and conversion of a linearly polarized wave into a circularly polarized wave.

The large number of investigations addressing the electromagnetic properties of materials and nonconventional physical systems via optical phenomena, along with research on different non-linear electrodynamics theories, provides strong motivation to examine the optical effects that may emerge in systems governed by ModMax electrodynamics.

In this work, we investigate some optical signatures of the ModMax ED, such as the reflection properties based on the Goos-Hänchen and in the complex Kerr effect. To do this, we consider the approach of the ModMax ED in an electromagnetic background that modifies the dispersion relations of a wave propagating through the material medium. Thus, we determine the contributions due to ModMax's non-linearity in relation to refractive indices and evaluate their influence on optical effects. These aspects can provide insights into new investigations as a nonlinear optical medium.

This paper is outlined as follows. In the section II, we revisit the ModMax ED in the presence of an electromagnetic background field. In the section III, we study the propagation modes (III A) and phase shift (III B) of the ModMax in a magnetic background field. The section IV is dedicated to the Goos-Hänchen effect in ModMax ED in the presence of an external magnetic field. Afterwards, in the section V, we investigate the complex Kerr rotation when both the electric (E) and magnetic (B) backgrounds are present under the conditions of $B > E$ and $E > B$, respectively. Finally, we summarize our results in section VI.

We use the natural units $\hbar = c = 1$ with $4\pi\epsilon_0 = 1$, and the Minkowski metric signature adopted is $\eta^{\mu\nu} = \text{diag}(+1, -1, -1, -1)$. In natural units, the electric and magnetic fields have squared-energy mass dimension

where the conversion of Volt/m and Tesla (T) to the natural system is as follows: $1 \text{ Volt/m} = 2.27 \times 10^{-24} \text{ GeV}^2$ and $1 \text{ T} = 6.8 \times 10^{-16} \text{ GeV}^2$, respectively.

II. BASICS ON MODMAX ED IN AN ELECTROMAGNETIC BACKGROUND FIELD

In this section, we review some results obtained in the ref. [37]. The non-linear ModMax ED is governed by the Lagrangian density

$$\mathcal{L}_{MM}(\mathcal{F}_0, \mathcal{G}_0) = \cosh \gamma \mathcal{F}_0 + \sinh \gamma \sqrt{\mathcal{F}_0^2 + \mathcal{G}_0^2}, \quad (1)$$

where γ is a real parameter that satisfies the condition $\gamma \geq 0$, and it depends on the Lorentz- and gauge-invariant bilinears $\mathcal{F}_0 = -\frac{1}{4} F_{0\mu\nu}^2 = \frac{1}{2} (\mathbf{E}_0^2 - \mathbf{B}_0^2)$, and $\mathcal{G}_0 = -\frac{1}{4} F_{0\mu\nu} \tilde{F}_0^{\mu\nu} = \mathbf{E}_0 \cdot \mathbf{B}_0$.

The electromagnetic field strength tensor is $F_0^{\mu\nu} = \partial^\mu A_0^\nu - \partial^\nu A_0^\mu = (-E_0^i, -\epsilon^{ijk} B_0^k)$, whose dual tensor is $\tilde{F}_0^{\mu\nu} = \epsilon^{\mu\nu\alpha\beta} F_{0\alpha\beta}/2 = (-B_0^i, \epsilon^{ijk} E_0^k)$, which satisfies the equations without sources, *i.e.*, $\partial_\mu \tilde{F}_0^{\mu\nu} = 0$.

The electromagnetic background field is so introduced by the expansion of the 4-potential as $A_0^\mu(x) = a^\mu(x) + A_B^\mu(x)$, where a^μ is the photon propagating field, and A_B^μ is the background 4-potential, that in case of an uniform and constant background field satisfies the relation $A_B^\mu = -F_{B\mu\nu} x^\nu/2$. As consequence, the strength field tensor $F_0^{\mu\nu}$ is written as $F_0^{\mu\nu} = f^{\mu\nu} + F_B^{\mu\nu}$, where $f^{\mu\nu} = \partial^\mu a^\nu - \partial^\nu a^\mu = (-e^i, -\epsilon^{ijk} b^k)$ is the propagating electromagnetic field in the space-time, and $F_B^{\mu\nu} = (-E^i, -\epsilon^{ijk} B^k)$ is the electromagnetic background field, which we consider uniform and constant throughout this paper. For convenience, the index (B) in the tensors is related with the EM background field.

Since we are interested in propagation effects, the Lagrangian (1) expanded up to second order in the propagating tensor $f^{\mu\nu}$ is

$$\mathcal{L}_{MM}^{(2)} = -\frac{1}{4} c_1 f_{\mu\nu}^2 - \frac{1}{4} c_2 f_{\mu\nu} \tilde{f}^{\mu\nu} + \frac{1}{8} Q_{B\mu\nu\kappa\lambda} f^{\mu\nu} f^{\kappa\lambda}, \quad (2)$$

where the background tensor $Q_{B\mu\nu\kappa\lambda}$ is defined by

$$Q_{B\mu\nu\kappa\lambda} = d_1 F_{B\mu\nu} F_{B\kappa\lambda} + d_2 \tilde{F}_{B\mu\nu} \tilde{F}_{B\kappa\lambda} + d_3 F_{B\mu\nu} \tilde{F}_{B\kappa\lambda} + d_3 \tilde{F}_{B\mu\nu} F_{B\kappa\lambda}, \quad (3)$$

and $\tilde{F}_B^{\mu\nu} = \epsilon^{\mu\nu\alpha\beta} F_{B\alpha\beta}/2 = (-B^i, \epsilon^{ijk} E^k)$ is the dual tensor of $F_{B\mu\nu}$. The coefficients c_1, c_2, d_1, d_2 and d_3 for the expansion from (2) are evaluated at the background fields \mathbf{E} and \mathbf{B} as:

$$\begin{aligned} c_1 &= \left. \frac{\partial \mathcal{L}_{MM}}{\partial \mathcal{F}_0} \right|_{\mathbf{E}, \mathbf{B}}, \quad c_2 = \left. \frac{\partial \mathcal{L}_{MM}}{\partial \mathcal{G}_0} \right|_{\mathbf{E}, \mathbf{B}}, \quad d_1 = \left. \frac{\partial^2 \mathcal{L}_{MM}}{\partial \mathcal{F}_0^2} \right|_{\mathbf{E}, \mathbf{B}}, \\ d_2 &= \left. \frac{\partial^2 \mathcal{L}_{MM}}{\partial \mathcal{G}_0^2} \right|_{\mathbf{E}, \mathbf{B}}, \quad d_3 = \left. \frac{\partial^2 \mathcal{L}_{MM}}{\partial \mathcal{F}_0 \partial \mathcal{G}_0} \right|_{\mathbf{E}, \mathbf{B}}. \end{aligned} \quad (4)$$

These coefficients depend only on the EM field magnitude, and also depend on the ModMax γ -parameter. Using the lagrangian density (1), the coefficients are given by

$$\begin{aligned} c_1 &= \cosh \gamma + \frac{\sinh \gamma \mathcal{F}}{\sqrt{\mathcal{F}^2 + \mathcal{G}^2}}, \quad c_2 = \frac{\sinh \gamma \mathcal{G}}{\sqrt{\mathcal{F}^2 + \mathcal{G}^2}}, \\ d_1 &= \frac{\sinh \gamma \mathcal{G}^2}{(\mathcal{F} + \mathcal{G}^2)^{3/2}}, \quad d_2 = \frac{\sinh \gamma \mathcal{F}^2}{(\mathcal{F}^2 + \mathcal{G}^2)^{3/2}}, \\ d_3 &= \frac{\sinh \gamma \mathcal{F} \mathcal{G}}{(\mathcal{F}^2 + \mathcal{G}^2)^{3/2}}, \end{aligned} \quad (5)$$

in which $\mathcal{F} = (\mathbf{E}^2 - \mathbf{B}^2)/2$ and $\mathcal{G} = \mathbf{E} \cdot \mathbf{B}$ are the gauge and Lorentz invariants related to \mathbf{E} and \mathbf{B} . Notice that in the particular case where the electric background is perpendicular to the magnetic one, $\mathcal{G} = \mathbf{E} \cdot \mathbf{B} = 0$, the coefficients are simplified as: $c_2 = d_1 = d_3 = 0$, and

$$c_1 = \cosh \gamma + \text{sgn}(\mathcal{F}) \sinh \gamma, \quad d_2 = \sinh \gamma \frac{\mathcal{F}^2}{|\mathcal{F}|^3}, \quad (6)$$

where $\text{sgn}(\mathcal{F})$ is the sign function of \mathcal{F} , with $\text{sgn}(\mathcal{F}) = +1$, if $\mathcal{F} > 0$, and $\text{sgn}(\mathcal{F}) = -1$, if $\mathcal{F} < 0$. The expressions (6) is the hardest case that leads in the paper for our analysis of optics effects.

Under these conditions, the field equations for the Lagrangian (2) are read as

$$\partial^\mu \left[c_1 f_{\mu\nu} - \frac{d_2}{2} \tilde{F}_{B\mu\nu} \left(\tilde{F}_{B\kappa\lambda} f^{\kappa\lambda} \right) \right] = 0, \quad (7a)$$

$$\partial_\mu \tilde{f}^{\mu\nu} = 0. \quad (7b)$$

In the vector form, the previous equations are

$$\nabla \cdot \mathbf{D} = 0, \quad \nabla \times \mathbf{e} + \frac{\partial \mathbf{b}}{\partial t} = \mathbf{0}, \quad (8a)$$

$$\nabla \cdot \mathbf{b} = 0, \quad \nabla \times \mathbf{H} - \frac{\partial \mathbf{D}}{\partial t} = \mathbf{0}, \quad (8b)$$

where the vectors \mathbf{D} and \mathbf{H} have the components

$$D_i = \epsilon_{ij} e_j + \sigma_{ij} b_j, \quad (9a)$$

$$H_i = -\sigma_{ji} e_j + (\mu^{-1})_{ij} b_j, \quad (9b)$$

that define the electric permittivity tensor ϵ_{ij} , σ_{ij} , and the inverse of the magnetic permeability tensor

$$\epsilon_{ij} = \delta_{ij} + d_E B_i B_j, \quad (10a)$$

$$\sigma_{ij} = d_E B_i E_j, \quad (10b)$$

$$(\mu^{-1})_{ij} = \delta_{ij} - d_E E_i E_j. \quad (10c)$$

Here, for simplicity, we have defined $d_E = d_2/c_1$. The usual Maxwell ED is recovered when $\gamma \rightarrow 0$.

Using the plane wave solutions for \mathbf{e} and \mathbf{b} , the equations (8a)-(8b) yield the wave equation for the electric amplitude \mathbf{e}_0 :

$$M^{ij} \mathbf{e}_0^j = 0, \quad (11)$$

where the matrix elements M^{ij} are given by

$$\begin{aligned} M^{ij} &= a \delta^{ij} + b n^i n^j + d_E B^i B^j \\ &\quad - d_E \mathbf{n}^2 E^i E^j + d_E (\mathbf{E} \cdot \mathbf{n}) (E^i n^j + E^j n^i) \\ &\quad + d_E \left[B^i (\mathbf{E} \times \mathbf{n})^j + B^j (\mathbf{E} \times \mathbf{n})^i \right], \end{aligned} \quad (12)$$

with $a = 1 - \mathbf{n}^2 + d_E (\mathbf{n} \times \mathbf{E})^2$ and $b = 1 - d_E \mathbf{E}^2$, and we have defined the refractive index as $\mathbf{n} = \mathbf{k}/\omega$, for a wave vector \mathbf{k} and wave frequency ω .

The non-trivial solution of (11) is when $\det(M_{ij}) = 0$. Thus, this polynomial equation provides three solutions: $n_1 = 1$ that confirms the gauge invariance of the model, $n_3 = 1$ in which we have $d_B = 0$ for electric and magnetic backgrounds perpendiculars, and the others solutions that we are interested in this paper are given by

$$n_{2EB}^{(\pm)} = \frac{1 + d_E \mathbf{B}^2}{d_E \mathbf{B} \cdot (\hat{\mathbf{k}} \times \mathbf{E}) \pm \sqrt{1 - d_E (\hat{\mathbf{k}} \times \mathbf{E})^2 - d_E^2 (\mathbf{E}^2 - \mathbf{B}^2) (\hat{\mathbf{k}} \cdot \mathbf{B})^2 + d_E (\hat{\mathbf{k}} \cdot \mathbf{B})^2 + d_E \mathbf{B}^2}}. \quad (13)$$

These last solutions provide the non-linear effects that we are interested for investigations through the Optics effects, as the phase shift, the Goos-Hänchen and the complex Kerr rotation.

III. PROPAGATING MODES AND PHASE SHIFT WITH MAGNETIC BACKGROUND

For the analysis of the propagating modes and phase shift, we consider only the magnetic background field,

that is, in the solutions of the previous section, we make $\mathbf{E} = \mathbf{0}$. In this case, the coefficients c_1 and d_2 are

$$c_1 = e^{-\gamma} \quad \text{and} \quad d_2 = 2 \frac{\sinh \gamma}{\mathbf{B}^2}, \quad (14)$$

in which d_E is

$$d_E = \frac{d_2}{c_1} = 2 e^\gamma \frac{\sinh \gamma}{\mathbf{B}^2} = \frac{e^{2\gamma} - 1}{\mathbf{B}^2}. \quad (15)$$

The non-trivial solutions of the refractive index in (13) reduces to :

$$n_{2B}^2 = \frac{1 + d_E \mathbf{B}^2}{1 + d_E (\mathbf{B} \cdot \hat{\mathbf{k}})^2} = \frac{e^{2\gamma}}{\sin^2 \theta + e^{2\gamma} \cos^2 \theta}, \quad (16)$$

that does not depend on the magnetic field magnitude, but it depends on the θ -angle that \mathbf{B} does with the wave propagation direction \mathbf{k} , in which $\cos \theta = \hat{\mathbf{k}} \cdot \hat{\mathbf{B}}$. The refractive index n_{1B} corresponds to the standard mode. On the other hand, the indices n_{2B} include all the anisotropic contributions and the ModMax γ -parameter. As indi-

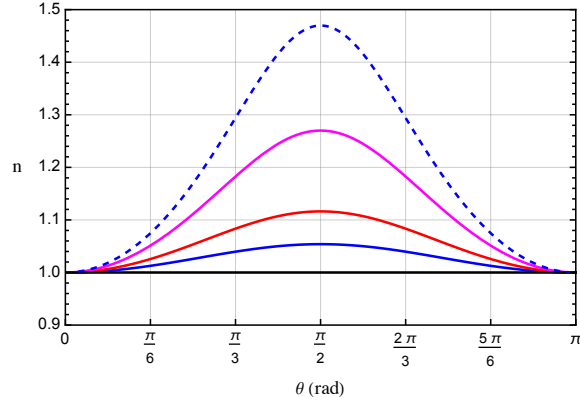


FIG. 1. Refractive index n_{2B} of Eq. (16) in terms of propagation direction θ . Here, we have set: $\gamma = 0.1$ (blue), 0.2 (red), 0.4 (magenta), 0.6 (dashed blue). The solid black curve represents the standard case with $\gamma \rightarrow 0$.

cated in the Fig. 1, the maximum values of refractive index n_{2B} happen when the direction of propagation is perpendicular to the background magnetic field, which means that birefringence effects can be enhanced when the magnetic field is perpendicular to the direction of light in the system. Furthermore, for propagation directions aligned to the magnetic field, that is, $\theta = \{0, \pi\}$, one finds $n_{2B} \rightarrow 1$, recovering the usual case.

We apply this result in the propagating modes ahead.

A. Propagating modes

To determine the polarizations of the propagating modes, let us choose a coordinate system in which $\mathbf{B} = (0, 0, B)$ and $\mathbf{n} = n(\sin \theta, 0, \cos \theta)$. Thereby, by considering particular these cases for propagation direction and implementing the previous solutions for the refractive indices, n_{1B} and n_{2B} , in Eq. (11), one finds that :

- i) For oblique directions of propagation with $\mathbf{n} = n(\sin \theta, 0, \cos \theta)$, with $\theta \neq \{0, \pi/2, \pi\}$, the propagating modes are

$$n_{1B} = 1, \quad \mathbf{e}_{1B} = \begin{pmatrix} 0 \\ 1 \\ 0 \end{pmatrix}, \quad (17)$$

and

$$n_{2B}^2 = \frac{e^{2\gamma}}{\sin^2 \theta + e^{2\gamma} \cos^2 \theta}, \quad (18a)$$

$$\mathbf{e}_{2B} = \frac{1}{\sqrt{1 + f^2}} \begin{pmatrix} 1 \\ 0 \\ -f \end{pmatrix}, \quad (18b)$$

where $f = e^{-2\gamma} \tan \theta$, and θ is the angle between $\hat{\mathbf{k}}$ and \mathbf{B} .

- ii) In Faraday configuration, $\mathbf{n} = (0, 0, n)$, ($\theta = 0, \pi$), it holds

$$n_{1B} = 1, \quad \mathbf{e}_{1B} = \frac{1}{\sqrt{1 + |a|^2}} \begin{pmatrix} 1 \\ a \\ 0 \end{pmatrix}, \quad (19)$$

$$n_{2B} = 1, \quad \mathbf{e}_{2B} = \frac{1}{\sqrt{1 + |a|^2}} \begin{pmatrix} 1 \\ b \\ 0 \end{pmatrix}, \quad (20)$$

with a and b being an arbitrary constants.

- iii) For Voigt configuration ($\theta = \pi/2$), one obtains

$$n_{1B} = 1, \quad \mathbf{e}_{1B} = \begin{pmatrix} 0 \\ 1 \\ 0 \end{pmatrix}, \quad (21)$$

$$n_{2B} = e^\gamma, \quad \mathbf{e}_{2B} = \begin{pmatrix} 0 \\ 0 \\ 1 \end{pmatrix}. \quad (22)$$

B. Phase shift

Let us consider the Faraday configuration given in item ii) of Sec. III A. In this case, the propagating modes related to n_{1B} and n_{2B+} are the same since $n_{1B} = n_{2B+}$, for which the polarization vector is given generically by the last relation in Eq. (17). On the other hand, for the propagating mode associated with n_{2B-} , one finds a linearly polarized vector. Thereby, the birefringence is evaluated in terms of the phase shift [56], defined by

$$\Delta = \frac{2\pi}{\lambda} d \Delta n, \quad (23)$$

where λ is the wavelength of the electromagnetic radiation in the vacuum, d corresponds to the thickness of the medium (or the distance the wave propagates through the medium), and Δn is the difference between the two refractive indices, that in this case is $\Delta n = n_{2B} - n_{1B}$. Therefore, one finds

Considering the Voigt configuration, we obtain the phase shift

$$\Delta = \frac{2\pi}{\lambda} d \left[\sqrt{1 + 2e^\gamma \sinh \gamma} - 1 \right] \simeq \frac{2\pi}{\lambda} d \gamma, \quad (24)$$

for a small γ -parameter.

IV. GOOS-HÄNCHEN EFFECT

We consider the interface between a simple dielectric, which we call medium 1, with electric permittivity ϵ_1 and magnetic permeability μ_1 , and medium 2 ruled by the ModMax electrodynamics. Considering the incident light coming from medium 1, and impinging on the surface of medium 2 with incidence angle θ_I greater than the critical angle θ_c , given by

$$\theta_c = \arcsin\left(\frac{n_{2B}}{\sqrt{\mu_1\epsilon_1}}\right). \quad (25)$$

where n_{2B} is the solution (16). The corresponding reflected wave can undergo a lateral shift, that is, a displacement of the reflected wave relative to the position in which there is no total reflection, defined by

$$D = -\frac{\lambda}{2\pi} \frac{\partial\varphi}{\partial\theta_I}, \quad (26)$$

where λ is the wavelength of the incident light, and φ is the phase acquired during the total reflection. This lateral optical shift of the reflected ray is known as the Goos-Hänchen shift [55, 57, 60]. We explore this effect in the situations in which the incident wave is *s*- and *p*-polarized.

1. Incident wave *s*-polarized

For an incident wave *s*-polarized, one can use $\mu_1 = \mu_2 = 1$, where the medium ruled by the ModMax electrodynamics in the magnetic background case, we have $\mu_2 = 1$, according to Eq. (10c), and $n_1 = \sqrt{\mu_1\epsilon_1}$ for the linear dielectric medium, which yields the following Fresnel coefficient

$$r_{2B}^s = \frac{\cos\theta_I - \sqrt{n_{2B}^2/\epsilon_1 - \sin^2\theta_I}}{\cos\theta_I + \sqrt{n_{2B}^2/\epsilon_1 - \sin^2\theta_I}}. \quad (27)$$

In the total reflection regime, it holds $\sin\theta_I > \sin\theta_c$, then Eq. (27) becomes

$$r_{2B}^s = e^{i\varphi_{2B}^s}, \quad (28)$$

where the phase is given by

$$\varphi_{2B}^s = -2 \arctan\left[\sec\theta_I \sqrt{\sin^2\theta_I - \frac{n_{2B}^2}{\epsilon_1}}\right]. \quad (29)$$

Substituting (29) in the definition (26), the Goos-Hänchen effect for *s*-wave polarized is

$$D_s = \frac{\lambda}{\pi} \sin\theta_I \left[\sin^2\theta_I - \frac{n_{2B}^2}{\epsilon_1}\right]^{-1/2}. \quad (30)$$

Notice that, in general, the result (30) is an implicit function of the γ -ModMax parameter and of the θ -angle of $\cos\theta = \hat{\mathbf{k}} \cdot \hat{\mathbf{B}}$ due to n_{2B} . For the Faraday configuration, we have $n_{2B} = 1$, the expression (30) is reduced to the simplest case :

$$D_s = \frac{\lambda}{\pi} \sin\theta_I \left[\sin^2\theta_I - \frac{1}{\epsilon_1}\right]^{-1/2}. \quad (31)$$

In the Voigt scenario, we obtain

$$D_s(\gamma) = \frac{\lambda}{\pi} \sin\theta_I \left[\sin^2\theta_I - \frac{e^{2\gamma}}{\epsilon_1}\right]^{-1/2}. \quad (32)$$

2. Incident wave *p*-polarized

For an incident wave *p*-polarized in the total reflection regime, we obtain

$$r_{2B}^p = e^{i\varphi_{2B}^p}, \quad (33)$$

with the reflection phase given by

$$\varphi_{2B}^p = -2 \arctan\left[\frac{\epsilon_1}{n_{2B}^2 \cos\theta_I} \sqrt{\sin^2\theta_I - \frac{n_{2B}^2}{\epsilon_1}}\right], \quad (34)$$

and using (26), we obtain

$$D_p = \frac{\lambda\epsilon_1}{\pi} \frac{n_{2B}^2 \sin\theta_I}{n_{2B}^4 \cos^2\theta_I - n_{2B}^2 \epsilon_1 + \epsilon_1^2 \sin^2\theta_I} \times \frac{1 - n_{2B}^2/\epsilon_1}{\sqrt{\sin^2\theta_I - n_{2B}^2/\epsilon_1}}. \quad (35)$$

In the Faraday configuration, we have

$$D_p = \frac{\lambda}{\pi} \frac{\sin\theta_I}{1 - \epsilon_1 + (\epsilon_1^2 - 1)\sin^2\theta_I} \frac{\epsilon_1 - 1}{\sqrt{\sin^2\theta_I - 1/\epsilon_1}}. \quad (36)$$

In the Voigt configuration, we obtain

$$D_p(\gamma) = \frac{\lambda\epsilon_1}{\pi} \frac{e^{2\gamma} \sin\theta_I}{e^{4\gamma} \cos^2\theta_I - e^{2\gamma}\epsilon_1 + \epsilon_1^2 \sin^2\theta_I} \times \frac{1 - e^{2\gamma}/\epsilon_1}{\sqrt{\sin^2\theta_I - e^{2\gamma}/\epsilon_1}}. \quad (37)$$

We illustrate the behavior of GH shift for *s*- and *p*-polarized incident waves in Fig. 2 as a function of incidence angle for configurations that depend on the γ parameter.

One observes that, in all cases illustrated, the GH effect assumes a large value for incidence angles greater than the critical angle of total reflection θ_c , which is given by

$$\theta_c = \arcsin\left[\frac{e^\gamma}{\sqrt{\epsilon_1}}\right], \quad (38)$$

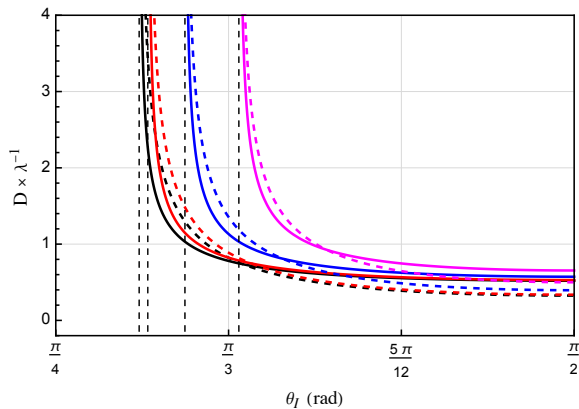


FIG. 2. Goos-Hänchen shift D_s of Eq. (32) for s -polarized incident wave (solid curves) and D_p of Eq. (37) (dashed lines) in terms of the incidence angle θ_I . Here, we have used: $\epsilon_1 = 1.6$, $\gamma = 0$ (usual scenario), 0.01 (red), 0.05 (blue), and 0.1 (magenta). The vertical dashed lines indicate the critical angle, given by Eq. (38), above which the GH effect takes place.

and then decreases monotonically toward its asymptotic value as the incidence angle approaches $\pi/2$. The standard scenario with $\gamma = 0$ is represented by the black lines in Fig. 2 for s -polarized incident wave (solid) and p -polarized incident wave (dashed).

Furthermore, for a fixed incidence angle, we observe that increasing the magnitude of the non-linear parameter γ yields an enhancement of the GH shift. In addition, the GH shift is slightly greater for p -polarized incident waves when the incidence angle is close to the critical angle θ_c .

It is important to mention that, since the GH effect takes place when total reflection occurs, one may establish a condition on the possible values of γ for which the GH effect can occur. In this sense, from $\sin \theta_I > \sin(e^\gamma/\sqrt{\epsilon_1})$ one finds

$$\gamma < \frac{1}{2} \ln(\epsilon_1 \sin^2 \theta_I), \quad (39)$$

and considering that the maximum value of $\sin \theta_I$ is unity, the γ parameter magnitude is constrained by

$$\gamma < \frac{1}{2} \ln(\epsilon_1). \quad (40)$$

The latter represents a condition on the magnitude of γ for which GH can take place.

In general, Figure 2 indicates that the GH effect is shifted from the usual cases (black lines) for both s - and

p -polarized incident waves. On the other hand, increasing the magnitude of γ parameter reduces the angular interval $\theta_c < \theta < \pi/2$ within which the effect is expected to occur.

V. COMPLEX KERR ROTATION

In this section, we consider the same situation: the interface between a linear dielectric medium, with electric permittivity ϵ_1 and magnetic permeability μ_1 , and the second medium ruled by the permittivity and permeability tensors of ModMax electrodynamics. We can now discuss the polarization aspects regarding the reflected wave scattered off from the surface of the exotic medium, whose nonlinear constitutive relations are given by (10a)-(10c) in the case in which the magnetic (\mathbf{B}) background field is perpendicular to the electric (\mathbf{E}) background. We will discuss the cases of $B > E$ and $E > B$.

A. The case $B > E$

Initially, we choose the condition of $B > E$, where the coefficients of the expansion around the EM background are reduced to

$$c_1 = e^{-\gamma}, \quad d_2 = \frac{2 \sinh \gamma}{B^2 - E^2}, \quad (41a)$$

$$c_2 = d_1 = d_3 = 0, \quad (41b)$$

$$d_B = 0, \quad d_E = \frac{e^{2\gamma} - 1}{B^2 - E^2}. \quad (41c)$$

In the case of incident light composed of s - and p -polarization states, e_\perp and e_\parallel , respectively, we can use the general results of complex Kerr rotation given in the Ref. [58], which allows us to write the reflection matrix equation as

$$\begin{pmatrix} e_R^\perp \\ e_R^\parallel \end{pmatrix} = \frac{1}{\Delta} \begin{pmatrix} r_{ss} & r_{sp} \\ r_{ps} & r_{pp} \end{pmatrix} \begin{pmatrix} e_\perp \\ e_\parallel \end{pmatrix}, \quad (42)$$

where e_R^\perp and e_R^\parallel are the s - and p -components of the reflected wave polarization.

We choose, for simplicity, the fields as $\mathbf{B} = B \hat{\mathbf{x}}$ and $\mathbf{E} = E \hat{\mathbf{z}}$, the wave propagation direction as $\mathbf{n}_2 = n_2 (\cos \theta, 0, \sin \theta)$ in the medium (2). Then implementing these conditions and the constitutive relations (10a)-(10c) in the reflection matrix (42), we obtain

$$\begin{pmatrix} e_{R\perp} \\ e_{R\parallel} \end{pmatrix} = \begin{pmatrix} \frac{\sqrt{\mu_1 \epsilon_1} \cos \theta_I - \mu_1 n_2 \cos \theta_T}{\sqrt{\mu_1 \epsilon_1} \cos \theta_I + \mu_1 n_2 \cos \theta_T} & \frac{2 \mu_1 \sqrt{\mu_1 \epsilon_1} d_E E B \cos \theta_I \sin \theta_I}{\Delta} \\ 0 & \frac{\mu_1 n_2 \cos \theta_I - \sqrt{\mu_1 \epsilon_1} \cos \theta_T}{\mu_1 n_2 \cos \theta_I + \sqrt{\mu_1 \epsilon_1} \cos \theta_T} \end{pmatrix} \begin{pmatrix} e_{\perp} \\ e_{\parallel} \end{pmatrix}, \quad (43)$$

with

$$\Delta = (\mu_1 n_2 \cos \theta_T + \sqrt{\mu_1 \epsilon_1} \cos \theta_I) (\mu_1 n_2 \cos \theta_I + \sqrt{\mu_1 \epsilon_1} \cos \theta_T), \quad (44)$$

in which θ_T is the refracted angle, and n_2 is the refractive index solution (13) with sign (+)

$$n_2^2 = \frac{B^2 e^{2\gamma} - E^2}{(B^2 - E^2) (\sin^2 \theta + e^{2\gamma} \cos^2 \theta)}, \quad (45)$$

which contains the dependence with the ModMax γ -parameter, and of the θ -angle. For an incident wave s -polarized, the complex Kerr rotation is described by the Kerr rotation angle θ_K , and the Kerr ellipticity angle η_K , given by

$$\tan(2\theta_K^s) = \frac{\text{Re}[2S]}{1 - |S|^2} \quad \text{and} \quad \sin(2\eta_K^s) = \frac{\text{Im}[2S]}{1 + |S|^2}, \quad (46)$$

where

$$S = \frac{r_{ps}}{r_{ss}}. \quad (47)$$

For the case of orthogonal electric and magnetic background fields (with $B > E$) in ModMax electrodynamics, the reflection matrix in Eq. (43) reveals that $S = 0$, meaning that $\theta_K^s = 0$ and $\eta_K^s = 0$. The latter indicates that the reflected wave is linearly polarized, while the former indicates that polarization rotation does not occur.

On the other hand, when the incident wave is p -polarized, the Kerr rotation angle, θ_K^p , and Kerr ellipticity angle, η_K^p , are given by

$$\tan(2\theta_K^p) = \frac{\text{Re}[2P]}{1 - |P|^2} \quad \text{and} \quad \sin(2\eta_K^p) = \frac{\text{Im}[2P]}{1 + |P|^2}, \quad (48)$$

where

$$P = \frac{r_{sp}}{r_{pp}}, \quad (49)$$

which reads

$$P = \frac{2 \sqrt{\frac{\epsilon_1}{\mu_1}} d_E E B \tan \theta_T}{n_2^2 - \frac{\epsilon_1}{\mu_1} + n_2 \sqrt{\frac{\epsilon_1}{\mu_1}} \chi}, \quad (50)$$

with

$$\chi = \frac{\cos \theta_I}{\cos \theta_T} - \frac{\cos \theta_T}{\cos \theta_I}. \quad (51)$$

The latter indicates that when incident light is p -polarized, the complex Kerr rotation takes place in the system. Notice that this effect takes place only when there are non-null electric and magnetic fields, which yields the mixed element r_{sp} in the reflection matrix of (43).

Considering the set chosen for external electromagnetic fields and propagation direction in medium 2 (nonlinear system ruled by ModMax electrodynamics), one can rewrite the θ angle in terms of transmission angle θ_T as $\theta = \pi/2 - \theta_T$. Afterwards, using Snell's law and the refractive index n_2 of Eq. (45), the transmission angle can be cast as

$$\theta_T = \arcsin \left[\sqrt{\frac{\mu_1 \epsilon_1 \sin^2 \theta_I (B^2 - E^2)}{B^2 e^{2\gamma} - E^2 + g (B^2 - E^2) \mu_1 \epsilon_1 \sin^2 \theta_I}} \right], \quad (52a)$$

with

$$g = 1 - e^{2\gamma}. \quad (52b)$$

To illustrate the characteristic Kerr rotation and Kerr ellipticity angles of Eq. (48), we implement Eq. (52) and Eq. (45) in Eq. (50), which yields

$$P|_{B>E} = \frac{-2 y (e^{2\gamma} - 1) \sqrt{\frac{\epsilon_1}{\mu_1}} Q_1}{(y^2 - 1) \left[\frac{(e^{2\gamma} - 1) \mu_1 \epsilon_1 (y^2 - 1) \sin^2 \theta_I - y^2 e^{2\gamma} + 1}{y^2 - 1} + Q_2 \right]}, \quad (53)$$

with

$$Q_1 = \sqrt{\frac{\mu_1 (y^2 - 1) \epsilon_1 \sin^2 \theta_I}{e^{2\gamma} \mu_1 (1 - y^2) \epsilon_1 \sin^2 \theta_I + e^{2\gamma} y^2 - 1}}, \quad (54a)$$

$$Q_2 = \frac{\epsilon_1}{\mu_1} + \frac{1 - y^2 e^{2\gamma} - \mu_1 \epsilon_1 g (y^2 - 1) \sin^2 \theta_I}{y^2 - 1} + Q_3, \quad (54b)$$

$$Q_3 = \frac{\sin \theta_I \sqrt{\frac{\epsilon_1}{\mu_1}} Q_6 \tan \theta_I Q_4}{2(y^2 - 1) Q_5 \sqrt{e^{2\gamma} y^2 - 1}}, \quad (54c)$$

$$Q_4 = \sqrt{\frac{(y^2 - 1) (e^{2\gamma} y^2 - 1)}{e^{2\gamma} y^2 - 1 + g \mu_1 \epsilon_1 (y^2 - 1) \sin^2 \theta_I}}, \quad (54d)$$

$$Q_5 = \sqrt{\frac{1 - e^{2\gamma} y^2 + e^{2\gamma} \mu_1 \epsilon_1 (y^2 - 1) \sin^2 \theta_I}{1 - e^{2\gamma} y^2 - g \mu_1 \epsilon_1 (y^2 - 1) \sin^2 \theta_I}}, \quad (54e)$$

$$Q_6 = -2(1 - e^{2\gamma} y^2) - \mu_1 \epsilon_1 (y^2 - 1) [1 + e^{2\gamma} + g \cos(2\theta_I)], \quad (54f)$$

where we have defined $y = B/E$.

In Fig. 3, we depict the Kerr rotation angle θ_K of Eq. (48) in terms of the incidence angle θ_I for some values of the dimensionless parameter $y = B/E$.

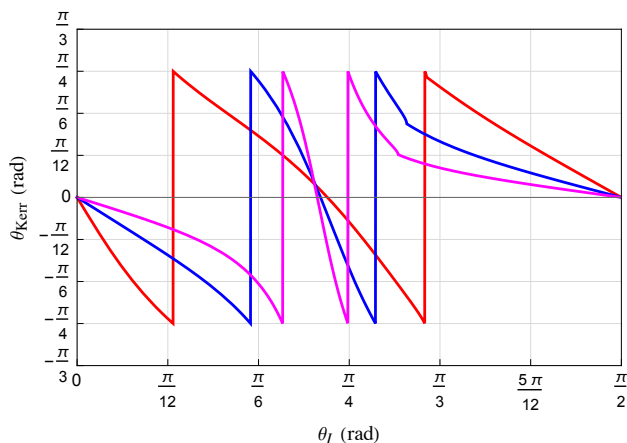


FIG. 3. Kerr rotation angle θ_K of Eq. (48) in terms of the incidence angle θ_I . Here, we have used: $\gamma = 0.1$, $\mu_1 = 1$, $\epsilon_1 = 1.6$, and $y = 1.5$ (red), 2 (blue), and 3 (magenta).

We note that in each example there are two abrupt changes in the sign of θ_K . This happens when $1 - |P|^2 \rightarrow 0$, which yields a divergence in the expression of θ_K . This sign change (or reversion) indicates, in general, that the major axis of the elliptically polarized reflected wave will change its rotation direction since $\theta_K > 0$ (< 0) means counterclockwise (clockwise) direction rotation [59, 61]. A similar behavior is also expected to occur in Weyl semimetals [51], whose electromagnetic response can be described within the axion electrodynamics framework. However, since the latter systems are dispersive, their abrupt sign change occur for specific frequencies, whereas for the nonlinear medium described in this work the sign change occurs at specific values of incidence angles θ_I which are obtained by solving the equation $1 - |P|^2 = 0$

for θ_I in each particular case. Furthermore, as the ratio $y = B/E$ increases, the values of θ_I in which the abrupt sign change occurs progressively approach each other.

The general behavior of Kerr ellipticity angle η_K of Eq. (48) is depicted in Fig. 4 in terms of the incidence angle θ_I for some values of $y = B/E$.

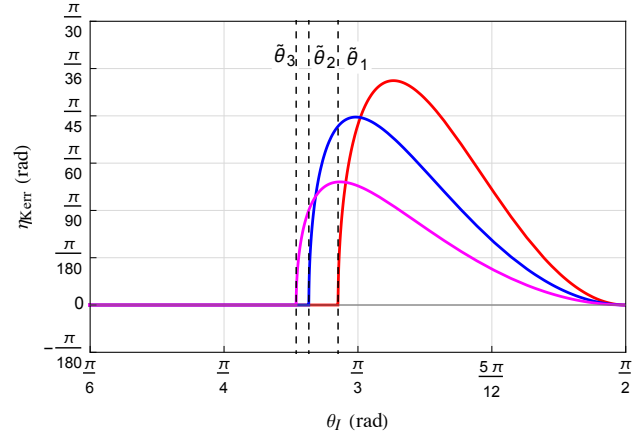


FIG. 4. Kerr ellipticity angle η_K of Eq. (48) in terms of the incidence angle θ_I . Here, we have used: $\gamma = 0.1$, $\mu_1 = 1$, $\epsilon_1 = 1.6$, and $y = 1.5$ (red), 2 (blue), and 3 (magenta). The vertical dashed lines are given by $\tilde{\theta}_i$ of Eq. (55) for each example $i = 1$ (red), 2 (blue), 3 (magenta).

The non-null values of η_K occur for $\theta_I > \tilde{\theta}_i$, where $\tilde{\theta}_i$ is given by

$$\tilde{\theta}_i = \arcsin \left[\sqrt{\frac{y^2 - e^{2\gamma}}{\mu_1 \epsilon_1 (y^2 - 1)}} \right], \quad (55)$$

considering $\gamma > 0$, $\mu_1 > 0$ and $\epsilon_1 > 0$. For the particular case with $\mu_1 = \epsilon_1 = 1$, one finds $\eta_K = 0$. The non-null values of η_K occurring for $\theta_I > \tilde{\theta}_i$ indicate that the reflected wave will be left-handed elliptically¹ polarized ($\eta_K > 0$). For $\theta_I < \tilde{\theta}_i$, the reflected wave is linearly polarized.

One observes that, as $y = B/E$ increases, the peak value of η_K decreases. Moreover, the value of $\tilde{\theta}_i$ also decreases, indicating that Kerr ellipticity arises over a wider range of incidence angles, which may be referred to as the *elliptical incidence window* $\theta_I > \tilde{\theta}_i$, meaning a range of incidence angles for which the reflected wave becomes elliptically polarized.

It is worth mentioning that the magnitude of Kerr rotations is typically small, being less than 1 degree in usual materials [50] and of the order 10^{-6} to 10^{-4} radians in topological insulators [51]. Thus, the values obtained here can be regarded as *giant* in comparison with those material systems.

¹ We are considering standard sign convention [59–61].

Another feature one notices is that, in Fig. 3, there is an incidence angle $\bar{\theta}_I$, defined in $\theta_{I(1)} < \bar{\theta}_{I(1)} < \theta_I$ (with $\theta_{I(1)}$ and $\theta_{I(2)}$ being solutions of $1 - |P|^2 = 0$) where occurs a smooth sign reversion of Kerr rotation angle. One may interpret this sign change as a reversion in the polarization rotation of a linearly polarized reflected wave when the Kerr ellipticity angle η_K is null. This means that, when $\eta_K = 0$, the reflected wave will be rotated to the left or to the right depending on the value of incidence angle θ_I , which can be found in two scenarios: *i*) $\bar{\theta}_{I(1)} < \theta_I < \bar{\theta}_I$, a linearly polarized reflected wave rotated in the counterclockwise direction (left); and *ii*) $\bar{\theta}_I < \theta_I < \bar{\theta}_{I(2)}$, the reflected wave will be rotated in the clockwise direction (right). Although an analytical expression for $\bar{\theta}_I$ seems difficult to be obtained since the expression of P in Eq. (53) is very complicated and intricate, one can obtain the value of $\bar{\theta}_I$, for each example in Fig. 3, by solving the equation

$$-g \mu_1 \epsilon_1 (y^2 - 1) \sin^2 \theta_I - y^2 e^{2\gamma} + 1 + (y^2 - 1) Q_2 = 0, \quad (56)$$

whose solution is

$$\theta_I = \arcsin \left[\sqrt{\frac{1 - Q_2 + y^2 (Q_2 - e^{2\gamma})}{g \mu_1 \epsilon_1 (y^2 - 1)}} \right]. \quad (57)$$

B. The case $E > B$

In this case of $E > B$, the coefficients of the expansion are given by

$$c_1 = e^\gamma, \quad (58a)$$

$$c_2 = d_1 = d_3 = 0, \quad (58b)$$

$$d_B = 0, \quad d_E = \frac{1 - e^{-2\gamma}}{E^2 - B^2}, \quad (58c)$$

in which the refractive index solution for $\mathbf{B} = B \hat{\mathbf{x}}$, $\mathbf{E} = E \hat{\mathbf{z}}$, and $\mathbf{n}_2 = n_2 (\cos \theta, 0, \sin \theta)$ in the medium (2) is

$$n_2^2 = \frac{E^2 e^{2\gamma} - B^2}{(E^2 - B^2)(e^{2\gamma} \sin^2 \theta + \cos^2 \theta)}. \quad (59)$$

Analogously to the procedure of the previous section, one finds now the refractive angle

$$\theta_T = \arcsin \left[\sqrt{\frac{\mu_1 \epsilon_1 \sin^2 \theta_I (E^2 - B^2)}{E^2 e^{2\gamma} - B^2 - g (E^2 - B^2) \mu_1 \epsilon_1 \sin^2 \theta_I}} \right], \quad (60)$$

with g defined in Eq. (52b).

Implementing Eq. (60) and Eq. (59) in Eq. (50), we obtain

$$P|_{E>B} = \frac{-2(e^{-2\gamma} - 1)x \sqrt{\frac{\epsilon_1}{\mu_1}} U_1}{(x^2 - 1)(U_2 + U_6)}, \quad (61)$$

where

$$U_1 = \sqrt{\frac{\mu_1 \epsilon_1 (x^2 - 1) \sin^2 \theta_I}{x^2 e^{2\gamma} - 1 - \mu_1 \epsilon_1 e^{2\gamma} (x^2 - 1) \sin^2 \theta_I}}, \quad (62a)$$

$$U_2 = -\frac{\epsilon_1}{\mu_1} + U_3, \quad (62b)$$

$$U_3 = \frac{2(-1 + x^2 e^{2\gamma}) U_4}{(y^2 - 1)(2e^{2\gamma} - 2e^{4\gamma} x^2 + U_5)}, \quad (62c)$$

$$U_4 = 1 - x^2 e^{2\gamma} - g \mu_1 \epsilon_1 (x^2 - 1) \sin^2 \theta_I, \quad (62d)$$

$$U_5 = (-1 - e^{2\gamma} + 2e^{4\gamma}) \mu_1 \epsilon_1 (x^2 - 1) \sin^2 \theta_I, \quad (62e)$$

$$U_6 = \frac{\sqrt{\frac{\epsilon_1}{2\mu_1}} \sin \theta_I \tan \theta_I \sqrt{x^2 e^{2\gamma} - 1} U_7 U_8}{[1 - x^2 e^{2\gamma} + e^{2\gamma} \mu_1 \epsilon_1 (x^2 - 1) \sin^2 \theta_I] U_9}, \quad (62f)$$

$$U_7 = -2 + 2x^2 e^{2\gamma} - (x^2 - 1) \mu_1 \epsilon_1 [1 + e^{2\gamma} + g \cos(2\theta_I)], \quad (62g)$$

$$U_8 = \sqrt{\frac{1 - x^2 e^{2\gamma} + e^{2\gamma} \mu_1 \epsilon_1 (x^2 - 1) \sin^2 \theta_I}{1 - x^2 e^{2\gamma} - g \mu_1 \epsilon_1 (x^2 - 1) \sin^2 \theta_I}}, \quad (62h)$$

$$U_9 = \sqrt{\frac{(x^2 - 1)(2e^{2\gamma} - 2x^2 e^{4\gamma} + U_{10})}{1 - x^2 e^{2\gamma} - g \mu_1 \epsilon_1 (x^2 - 1) \sin^2 \theta_I}}, \quad (62i)$$

$$U_{10} = \mu_1 \epsilon_1 (x^2 - 1)(-1 - e^{2\gamma} + 2e^{4\gamma}) \sin^2 \theta_I. \quad (62j)$$

Using now Eq. (61), we illustrate the general behavior of θ_K in terms of incidence angle θ_I in Fig. 5 for some values of the dimensionless parameter $x = E/B$.

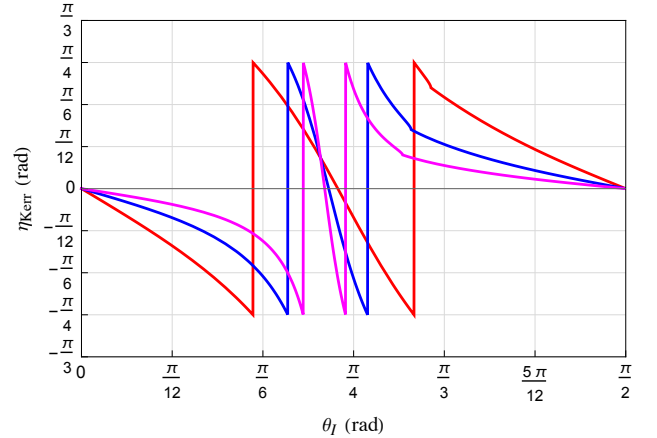


FIG. 5. Kerr rotation angle θ_K of Eq. (48) in terms of the incidence angle θ_I . Here, we have used: $\gamma = 0.1$, $\mu_1 = 1$, $\epsilon_1 = 1.6$, and $x = 1.5$ (red), 2 (blue), and 3 (magenta).

As before, one also notices that there are two abrupt sign changes for θ_K , which occur at incidence angles $\bar{\theta}_I$ that are solutions of $1 - |P|^2 = 0$ with P of Eq. (61). Moreover, as $x = E/B$ increases, the two divergences approach each other progressively. On the other hand, for $E > B$, these two angles are closer to each other when compared to the case of $B > E$ for the same set of electromagnetic parameters.

Regarding the Kerr ellipticity, for $E > B$ the peak of η_K is smaller in comparison with $B > E$ scenario, as

shown in Fig. 6. This means that the polarization ellipse of the reflected wave is more eccentric than that expected in the scenario of $B > E$. The elliptical incidence window in this case is defined by $\theta_I > \hat{\theta}_i$, with $\hat{\theta}_i$ given by

$$\hat{\theta}_i = \arcsin \left[\sqrt{\frac{x^2 - e^{2\gamma}}{\mu_1 \epsilon_1 (x^2 - 1)}} \right], \quad (63)$$

in which i -index ($i = 1, 2, 3$) symbols the colors red, blue, and magenta in the Fig. 6.

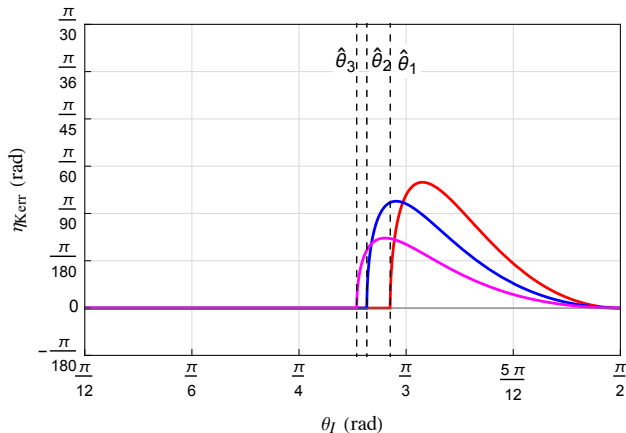


FIG. 6. Kerr ellipticity angle η_K of Eq. (48) in terms of the incidence angle θ_I . Here, we have used: $\gamma = 0.1$, $\mu_1 = 1$, $\epsilon_1 = 1.6$, and $x = 1.5$ (red), 2 (blue), and 3 (magenta). The vertical dashed lines indicate the incidence angle $\hat{\theta}_i$ of Eq. (63).

VI. FINAL REMARKS

In this work, we have investigated some optical properties arising in systems ruled by the modified Maxwell (ModMax) electrodynamics. First, we have obtained the general dispersion relations and modified refractive indices considering uniform external electric and magnetic backgrounds. In the case of a uniform magnetic background, the modified refractive index presents a θ dependence, which represents the angle between the direction of propagation and the magnetic background. In this scenario, the propagating modes are, generally, given by linearly polarized vectors. Thereby, the birefringence can be evaluated in terms of phase shift of Eq. (24), which has linear dependence on the non-linear ModMax γ -parameter, in the limit of small γ .

Regarding reflection properties, we have also investigated the Goos-Hänchen (GH) shift in the scenario

of a uniform magnetic background in Sec. IV. For s -polarized incident wave, the GH effect is given, generally, by Eq. (30), whereas for p -polarized incident wave, the GH shift is given by Eq. (35).

To investigate the Kerr rotation, we have considered the case with perpendicular uniform electric (E) and magnetic (B) background fields with $B > E$ and $E > B$ in Sec. V. In the scenario of $B > E$, one finds that for s -polarized incident wave, the Kerr rotation angle (θ_K) and Kerr ellipticity (η_K) are null, regardless of the magnitude of background fields and non-linear parameter γ . On the other hand, for p -polarized incident wave, Kerr rotation takes place for oblique incidence angles θ_I and $\gamma > 0$, as indicated in Eq. (53). The abrupt sign change of θ_K happens for specific incidence angles $\tilde{\theta}_I$ obtained by solving $1 - |P|^2 = 0$, with P given by Eq. (53). This abrupt sign change is also expected to occur in Weyl semimetals, whose electromagnetic response is described by the axion electrodynamics. In such a scenario, the axion terms yield the Kerr rotation. In the case investigated in this work, however, the Kerr signals occur due to a non-null uniform electromagnetic background and the non-linear parameter γ .

Furthermore, Kerr ellipticity angle η_K assumes non-null values for $\theta_I > \tilde{\theta}_i$, with $\tilde{\theta}_i = \arcsin \left[\sqrt{\frac{y^2 - e^{2\gamma}}{\mu_1 \epsilon_1 (y^2 - 1)}} \right]$, and $y = B/E$, which may be regarded as the elliptical incidence window, *i. e.*, the reflected wave becomes elliptically polarized when the incidence angle lies within the range $\theta_I > \tilde{\theta}_i$. This feature may work as a polarization conversion mechanism: p -polarized incident wave may be transformed into a left-handed elliptically polarized wave by reflecting on a non-usual medium ruled by the ModMax ED. In the particular cases where $\eta_K = 0$, the reflected wave remains linearly polarized.

In the regime $E > B$, the Kerr rotation angle θ_K and ellipticity η_K behave analogously to the case observed when $B > E$. However, the peak value of η_K for $E > B$ is smaller than that of $B > E$, meaning that the polarization ellipse for the reflected wave is more eccentric in this case. The corresponding elliptical incidence window is now defined by $\theta_I > \hat{\theta}_i$, with $\hat{\theta}_i = \arcsin \left[\sqrt{\frac{x^2 - e^{2\gamma}}{\mu_1 \epsilon_1 (x^2 - 1)}} \right]$, and $x = E/B$.

In general, our results show that the non-linear parameter γ , together with the quantities $y = B/E$ and $x = E/B$, play a key role in controlling the magnitude of Kerr signals (rotation and ellipticity), as well as the angular interval in which elliptically polarized light emerges. These properties suggest that ModMax electrodynamics can provide a consistent framework for investigating and describing non-usual material systems with optical effects induced by nonlinear electromagnetic effects.

Finally, we summarize some of the main properties obtained for non-usual medium ruled by ModMax electrodynamics in Tab. I.

TABLE I. Some optical effects in ModMax electrodynamics

Optical effect	
Birefringence	yes. Refractive indices are given by Eq. (13).
Propagation modes	Linearly polarized vectors for uniform magnetic background.
Goos-Hänchen shift	yes. The GH effect is given by Eq. (30) and Eq. (35) for s - and p -polarized incident waves, respectively. For p -polarized incident waves, the GH shift is slightly enhanced compared to GH for s -polarized waves.
Complex Kerr rotation	yes. It takes place for non-null electric and magnetic backgrounds and oblique incidence angles. For s -polarized incident wave, $\eta_K = 0$ and $\theta_K = 0$. For p -polarized incident wave, θ_K and η_K are given by Eq. (48) with P defined in two cases: i) P of Eq. (53) for $B > E$; ii) P of Eq. (61) for $E > B$.

ACKNOWLEDGEMENTS

The authors express their gratitude to FAPEMA, CNPq, and CAPES (Brazilian research agencies) for their invaluable financial support. P.D.S.S. is grateful to grant Produtividade/FAPEMA/CNPq/12649/25. Furthermore, we are indebted to CAPES/Finance Code 001.

-
- [1] R. Battesti and C. Rizzo, Magnetic and electric properties of a quantum vacuum, *Rep. Prog. Phys.* **76**, 016401 (2013).
 - [2] H. Euler and W. Heisenberg, Consequences of Dirac Theory of the Positron, *Z. Phys.* **98**, 714 (1936).
 - [3] V. S. Weisskopf, Über die elektrodynamik des vakuums auf grund des quanten-theorie des elektrons, *Dan. Mat. Fys. Medd.* **14**, 1 (1936).
 - [4] A. Ejlli, F. Della Valle, U. Gastaldi, G. Messineo, R. Pengo, G. Ruoso and G. Zavattini, The PVLAS experiment: A 25 year effort to measure vacuum magnetic birefringence, *Phys. Rep.* **871**, 1 (2020).
 - [5] G. Zavattini, U. Gastaldi, R. Pengo, G. Ruoso, F. Della Valle, and E. Milotti, Measuring the magnetic birefringence of vacuum: the PVLAS experiment, *Int. J. of Mod. Phys. A* **27**, 1260017 (2012).
 - [6] F. Della Valle, A. Ejlli, U. Gastaldi, G. Messineo, E. Milotti, R. Pengo, G. Ruoso and G. Zavattini, The PVLAS experiment: measuring vacuum magnetic birefringence and dichroism with a birefringent Fabry-Perot cavity, *Eur. Phys. J. C* **76**, 24 (2016).
 - [7] G. Zavattini and F. Della Valle, Optical polarimetry for fundamental physics, *Universe* **7** (7), 252 (2021).
 - [8] R. P. Mignani, V. Testa, D. Gonzalez Caniulef, R. Taverna, R. Turolla, S. Zane and K. Wu, Evidence for vacuum birefringence from the first optical polarimetry measurement of the isolated neutron star RX J1856.5-3754, *Monthly Notices of the Royal Astronomical Society* **465**, 1 (2017).
 - [9] M. Born and L. Infeld, Foundations of the new field theory, *Proc. R. Soc. Lond. Ser. A* **144**, 425 (1934).
 - [10] E. S. Fradkin and A. A. Tseytlin, Non-linear electrodynamics from quantized strings, *Phys. Lett. B* **163**, 123 (1985).
 - [11] E. Bergshoeff, E. Sezgin, C. N. Pope and P. K. Townsend, The Born-Infeld action from conformal invariance of the open superstring, *Phys. Lett. B* **188**, 70 (1987).
 - [12] R. Banerjee and D. Roychowdhury, Critical behavior of Born-Infeld AdS black holes in higher dimensions, *Phys. Rev. D* **85**, 104043 (2012).
 - [13] S. Gunasekaran, D. Kubiznak and R. B. Mann, Extended phase space thermodynamics for charged and rotating black holes and Born-Infeld vacuum polarization, *JHEP* **1211**, 110 (2012).
 - [14] Eloy Ayón-Beato and Alberto García, The Bardeen Model as a Nonlinear Magnetic Monopole, *Phys. Lett. B* **493**, 149-152 (2000).
 - [15] John Ellis, Nick E. Mavromatos and Tevong You, Light-by-Light Scattering Constraint on Born-Infeld Theory, *Phys. Rev. Lett.* **118**, 261802 (2017).
 - [16] Aydın Cem Keser, Yuli Lyanda-Geller, and Oleg P. Sushkov, Nonlinear Quantum Electrodynamics in Dirac Materials, *Phys. Rev. Lett.* **128**, 66402 (2022).
 - [17] E. M. Murchikova, On nonlinear classical electrodynamics with an axionic term, *J. Phys. A: Math. Theor.* **44**, 045401 (2011).
 - [18] J. M. A. Paixão, L. P. R. Ospedal, M. J. Neves, and J. A. Helayël-Neto, The axion-photon mixing in non-linear electrodynamic scenarios, *JHEP* **10**, 160 (2022).
 - [19] F. Haas, P. Gaete, L. P. R. Ospedal, and J. A. Helayël-Neto, Modified plasma waves described by a logarithmic electrodynamics, *Phys. Plasmas* **26** - 4, 042108 (2019).

- [20] L. P. R. Ospedal and F. Haas, Probing modified plasma waves in non-linear electrodynamics, *Phys. Plasmas* **30** - 6, 062112 (2023).
- [21] J. Plebanski, *Lectures on nonlinear electrodynamics*, Cycle of lectures delivered at The Niels Bohr Institute and NORDITA, Copenhagen, October 1968.
- [22] G. Boillat, Nonlinear electrodynamics: Lagrangian and equations of motion, *J. Math. Phys.* **11**, 941 (1970).
- [23] Z. Bialynicka-Birula and I. Bialynicki-Birula, Nonlinear effects in Quantum Electrodynamics. Photon propagation and photon splitting in an external field, *Phys. Rev. D* **2**, 2341 (1970).
- [24] I. Bialynicki-Birula, *Quantum Theory of Particles and Fields: birthday volume dedicated to Jan Lopuszański: Nonlinear Electrodynamics: Variations on a theme by Born and Infeld*, World Scientific, 1983, pp 31.
- [25] Dmitri P. Sorokin, Introductory Notes on Non-linear Electrodynamics and its Applications, *Fortschr. Phys.* **70**, 2200092 (2022).
- [26] H. Babaei-Aghbolagh, K.B Velni, D.M. Yekta, and H. Mohammadzadeh, Emergence of non-linear electrodynamic theories from $T\bar{T}$ -like deformations, *Phys. Lett. B* **829**, 137079 (2022).
- [27] H. Babaei-Aghbolagh, K.B Velni, D.M. Yekta and H. Mohammadzadeh, $T\bar{T}$ -like flows in non-linear electrodynamic theories and S-duality, *JHEP* **2021**,187 (2021).
- [28] P. Niau Akmansoy and L. G. Medeiros, Constraining Born-Infeld-like nonlinear electrodynamics using hydrogen's ionization energy, *Eur. Phys. J. C* **78**, 143 (2018).
- [29] P. Niau Akmansoy and L. G. Medeiros, Constraining nonlinear corrections to Maxwell electrodynamics using $\gamma\gamma$ scattering, *Phys. Rev. D* **99**, 115005 (2019).
- [30] M. J. Neves, J. B. de Oliveira, L. P. R. Ospedal and J. A. Helayël-Neto, Dispersion Relations in Non-Linear Electrodynamics and the Kinematics of the Compton Effect in a Magnetic Background, *Phys. Rev. D* **104**, 015006 (2021).
- [31] M. J. Neves, L. P. R. Ospedal, J. A. Helayël-Neto and Patricio Gaete, Considerations on anomalous photon and Z-boson self-couplings from the Born-Infeld weak hypercharge action, *Eur. Phys. J. C* **82**, 327 (2022).
- [32] I. Bandos, K. Lechner, D. Sorokin and P. T. Townsend, A non-linear duality-invariant conformal extension of Maxwell's equations, *Phys. Rev. D* **102**, 121703(R) (2020).
- [33] K. Lechner, P. Marchetti, A. Sainaghi and D. Sorokin, Maximally symmetric nonlinear extension of electrodynamics and charged particles, *Phys. Rev. D* **106**, 016009 (2022).
- [34] S. I. Kruglov, Magnetic black holes with generalized ModMax model of nonlinear electrodynamics, *Int. J. Mod. Phys. D* **31**: 04, 2250025 (2022).
- [35] I. Bandos, K. Lechner, D. Sorokin and P. K. Townsend, ModMax meets Susy, *JHEP* **10**, 031 (2021).
- [36] I. Bandos, K. Lechner, D. Sorokin and P. K. Townsend, Trirefringence and the M5-brane, *JHEP* **06**, 171 (2023).
- [37] M. J. Neves, P. Gaete, L. P. R. Ospedal, and J. A. Helayël-Neto, Considerations on the modified Maxwell electrodynamics in the presence of an electric and magnetic background, *Phys. Rev. D* **107**, 075019 (2023).
- [38] F. Goos and H. Hanchen, Ein neuer und fundamentaler Versuch zur Totalreflexion, *Annalen der Physik* **436** (7-8): 333-346 (1947).
- [39] S. Miller, Y. Ding, L. Jiang, Xingzhou Tu, S. Pau, Observation of elliptically polarized light from total internal reflection in bubbles, *Sci. Rep.* **10**, 8725 (2020).
- [40] Scott Robertson, Optical Kerr effect in vacuum, *Phys. Rev. A* **100**, 063831 (2019).
- [41] K. Sato and T. Ishibashi, Fundamentals of Magneto-Optical Spectroscopy, *Front. Phys.* **10**: 946515, (2022).
- [42] K. Shinagawa, in: Solid-State Sciences: Magneto-Optics, Vol. 128, Berlin: Springer-Verlag, 2000.
- [43] P. N. Argyles, Theory of the Faraday and Kerr Effects in Ferromagnetics, *Phys. Rev.* **97**, 334 (1955).
- [44] M. Kargarian, M. Randeria, and N. Trivedi, Theory of Kerr and Faraday rotations and linear dichroism in Topological Weyl Semimetals, *Sci. Rep.* **5**, 12683 (2015).
- [45] S. Ghosh, A. Sahoo, and S. Nandy, Theoretical investigations on Kerr and Faraday rotations in topological multi-Weyl semimetals, *SciPost Phys.* **15**, 133 (2023).
- [46] A. Sekine and K. Nomura, Axion electrodynamics in topological materials, *J. Appl. Phys.* **129**, 141101 (2021).
- [47] O. Trépanier, R. Duchesne, J. J. Boudreault, and R. Côté, Magneto-optical Kerr effect in Weyl semimetals with broken inversion and time-reversal symmetries, *Phys. Rev. B* **106**, 125104 (2022).
- [48] R. Côté, R. N. Duchesne, G. D. Duchesne, and O. Trépanier, Chiral filtration and Faraday rotation in multi-Weyl semimetals, *Results Phys.* **54**, 107064 (2023).
- [49] C. Guo, V. S. Asadchy, B. Zhao, and S. Fan, Light control with Weyl semimetals, *eLight* **3**, 2 (2023).
- [50] M. Schlenker and Y. Souche, in: Magnetism: Fundamentals, Boston (USA): Springer Science, 2005.
- [51] K. Sonowal, A. Singh, and A. Agarwal, Giant optical activity and Kerr effect in type-I and type-II Weyl semimetals, *Phys. Rev. B* **100**, 085436 (2019).
- [52] T. Li, Y. Wang, Y. Jiang, S. Zhang, L. Luo, and Z. Zhang, High-precision measurement of the complex magneto-optical Kerr effect using weak measurement, *Appl. Phys. Lett.* **124**, 054001 (2024).
- [53] A. Kapitulnik, J. Xia, E. Schemm, and A. Palevski, Polar Kerr effect as probe for time-reversal symmetry breaking in unconventional superconductors, *New J. Phys.* **11**, 055060 (2009).
- [54] A. M.-Ruiz and C. A. Escobar, Casimir effect between ponderable media as modeled by the standard model extension, *Phys. Rev. D* **94**, 076010 (2016).
- [55] P. D. S. Silva, R. A. Pereira, and M. M. Ferreira Jr., Optical reflection signature of an axion dielectric with magnetic current, *Phys. Rev. B* **110**, 174427 (2024).
- [56] P. D. S. Silva, L. Lisboa-Santos, M. M. Ferreira Jr., and M. Schreck, Effects of CPT -odd terms of dimensions three and five on electromagnetic propagation in continuous matter, *Phys. Rev. D* **104**, 116023 (2021).
- [57] Ming-Che Chang and Min-Fong Yang, Optical signature of topological insulators, *Phys. Rev. B* **80**, 113304 (2009).
- [58] P. D. S. Silva, A. Nonato, and M. M. Ferreira Jr., work in progress.
- [59] A. Zangwill, *Modern Electrodynamics*. New York (USA): Cambridge University Press, 2012.
- [60] J. D. Jackson, *Classical Electrodynamics*, 3rd edition. New York (USA): John Wiley & Sons, 1999.
- [61] E. Hecht, *Optics*, 4th ed. (Addison Wesley, San Francisco, 2002).